

Pressure and Temperature Dependent Dynamic Flow and Failure Behavior of PMMA at Intermediate Strain Rates

Longhui Zhang^{1*}, David Townsend¹, Nik Petrinic¹, Antonio Pellegrino¹

¹ Department of Engineering Science, University of Oxford, Parks Road, Oxford, OX1 3PJ, U.K.

*Corresponding author: longhui.zhang@eng.ox.ac.uk

Abstract:

Polymethylmethacrylate (PMMA) has been widely used as transparency in aerospace and automobile engineering to enhance structural reliability under impact loading such as bird strike events. This study investigates the confined compressive behaviour of PMMA at quasi-static 0.01 s^{-1} , medium rate $1\text{-}100 \text{ s}^{-1}$ and intermediate strain rates $100\text{-}1000 \text{ s}^{-1}$ from room temperature to elevated temperatures. Constant intermediate strain rate loading is achieved by using pulse shaping technique on a bespoke in-house developed split Hopkinson compression bar equipped with a high-speed camera and an environmental chamber. The material presents significant strain rate, temperature and pressure sensitivities. The failure mode at intermediate strain rate changes from brittle fragmentation without confinement to adiabatic shear banding with medium lateral confinement (65.3 MPa), which can be seen from the post-peak slope in the constitutive behavior, melting flow PMMA filaments observed in high speed photography and microstructural analysis. A series of intermediate strain rate experiments at elevated temperatures indicate that the higher temperature results in ductile failure for corresponding pressures. The temperature and strain rate dependent Drucker-Prager (DP) model is found to describe the response of PMMA. The brittle-ductile transition and pressure dependent model provide a better understanding of PMMA at intermediate strain rates, which is appropriate for engineering applications.

Keywords: PMMA, Intermediate strain rate, Confined compression, Pressure, Temperature, Hopkinson bar, Shear Localization

1. Introduction

PMMA, as a representative thermoplastic polymer, is increasingly employed in various aeronautical and structural engineering applications. The laminated structure consisting of two glass panels joined with a polymeric layer is typical transparency for windshield of car, high-speed train, and aircraft. Due to the excellent transparent property and high impact resistance, PMMA is of great interest as an intermediate layer in laminated windshield. The transparency subjected to impact events such as bird strike undergoes high-speed deformation processes [1, 2]. Investigation of the dynamic mechanical and failure behaviour of PMMA is important in order to ensure the structural integrity and passenger safety.

A large amount of efforts has been dedicated to measuring material properties of PMMA at high strain rates over 1000 s^{-1} in the past five decades. Kolsky [3] was the first to characterize the mechanical behaviour of PMMA at high rates of loading by using the split Hopkinson bar (later called Kolsky bar) and compared the dynamic and static stress-strain curves obtained from a hydraulic ram apparatus. Fleck et al. [4] studied the temperature dependent shear response of PMMA from 500 s^{-1} to 2200 s^{-1} by using a Hopkinson torsion bar, and found PMMA fractured before yield in the high strain rate tests for the temperatures less than the glass transition temperature. Richeton et al. [5] conducted the uniaxial compression tests at strain rates from 0.0001 s^{-1} to 10 s^{-1} and over 1000 s^{-1} at several temperatures. The mechanical response of PMMA was strongly affected by strain rate and temperature. Increasing temperature decreased yield stress and the strain hardening rate, whereas the increasing strain rate increased these two quantities. A key characteristic of dynamically deforming PMMA is related to thermomechanical coupling effects, in which the invested mechanical energy elevates the temperature of the deforming material. Rittel [6] quantitatively evaluated the adiabatic temperature rise in PMMA at a very high strain rate from 6500 s^{-1} to 7000 s^{-1} . This thermomechanical response was characteristic of that of the process zone material ahead of crack-tip. Recently, Kendall and Siviour [7] carried out a series of careful simulation experiments to investigate the nature of temperature dependent behaviour of PMMA at high strain rates. All high rate mechanical energy of PMMA was reproduced by using heat to stimulate the strain softening. From the literature, one can find a gap exists in the mechanical characterization of PMMA at the level of 10 s^{-1} - 1000 s^{-1} , which cannot be easily achieved with conventional specimens or testing equipment. *To better understand the constitutive response of PMMA, it is important to study the mechanical*

behaviour of PMMA over a wide range of strain rates (and temperatures) and fill this gap at the strain rate level of 10 s^{-1} - 1000 s^{-1} .

Being considered as a brittle material at high strain rates, PMMA tends to fragment readily. It's interesting to note the punch tests of PMMA plates carried out by Winter et al. [8], the deformation occurred in localized shear bands, which was similar to the deformation in loaded titanium plates due to the thermal softening effects. Later, Satapathy et al. [9] investigated the deep punching experiments on PMMA and reported that the application of proper lateral confinement suppressed the cracks, compared to the cracked specimens without lateral confinement. Recently, Rittel et al. [10] studied the static and dynamic response of confined PMMA and reported the pressure induced brittle–ductile transition at high strain rates over 2000 s^{-1} , in which the failure mode changed to adiabatic shear localization, instead of axial splitting and fragmentation. The confined behaviour of PMMA under quasi-static loading and at high strain rates of over 1000 s^{-1} was also investigated by Forquin et al. [11]. However, it was found that both unconfined and confined PMMA exhibited elastic brittle behaviour at high strain rates.

Regardless of the propensity to impact induced fragmentation, the confinement could potentially play a role in delaying the crack and brittle failure in dynamically deforming PMMA and would benefit the impact resistant windshield design. Yao et al. [12, 13] systematically studied the PMMA windshield subjected to soft body impact and reported that the PMMA material deformed in the intermediate strain rate region, less than several hundred per second, during impact events. The PMMA was subjected to dynamic compressive stresses with high pressure in the vicinity of the striking position. However, *the pressure effect on dynamic response of PMMA at this intermediate strain rate region is seldom studied.* In addition, the windshield components of aircraft and high-speed train in service undergo various temperature conditions. *The influence of temperature on confined PMMA, however, is still unknown.* Therefore, in the present paper, quasi-static, medium to intermediate strain rate compressive confined experiments, complemented by Digital Image Correlation (DIC) technique [14, 15], are conducted to measure the constitutive response of PMMA and understand the rate (and temperature) dependent dynamic failure modes. The experimental results will provide guidance for the design of impact resistance windshield applications.

The present work aims to study the effects of pressure and temperature on the compressive deformation and failure behaviour of PMMA across a wide range of strain rates, particularly

intermediate strain rates at the level of 100 s^{-1} which are difficult for both hydraulic machine and classical Hopkinson compression bar to achieve, under different temperature conditions. The paper is organized as follows: the material, specimen and the experimental setups are introduced in Section 2. The experimental results at various strain rates (and temperatures) are reported in Section 3. The next section introduces the constitutive modelling of pressure sensitivity of PMMA. Section 5 is the discussion and summary of the experimental data, following by conclusion remarks.

2. Experimental Protocol

2.1 Material and specimens

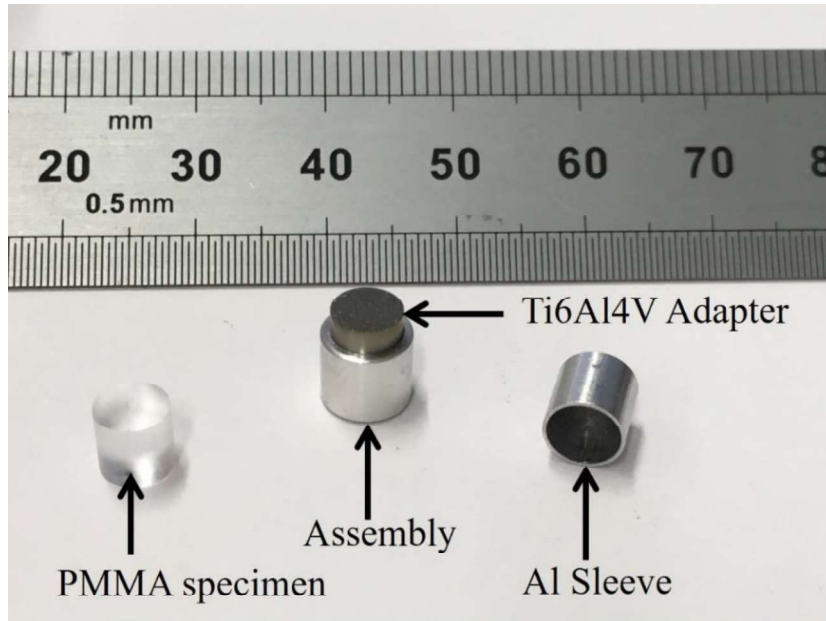
The cylindrical specimen with 5mm diameter and 5mm length were prepared from a 10 mm diameter PMMA rod, with density 1180 kg/m^3 and Rockwell hardness M90. The confinement was applied by a mechanical approach from a sleeve designed to be yield at the early stage of the experiment and with a low-strain hardening undergoing plastic deformation to obtain a constant pressure [10, 16]. Various levels of confined pressure were achieved by sleeves machined from Al 6061 with three different wall thicknesses 0.3 mm, 0.5 mm and 0.7 mm \pm 0.005 mm. The PMMA specimen, Al sleeve and the assembly are shown in Fig.1a, with a cylindrical Ti6Al4V alloy adapter on top of the confined specimen to complete the assembly. Grease lubricated PMMA specimen can be inserted tightly into Al sleeve with hand pressure (0.01 mm geometric tolerance between the sleeve and specimen), hence the friction between the Al sleeve and PMMA specimen is assumed to be negligible in the present paper. The relevant numerical studies to evaluate the influence of friction between the lubricated PMMA and the Al sleeve on the axial stress given in Appendix A. The specimen was loaded through the adapter by the load cell or the incident Hopkinson bar. The schematic diagram in Fig.1b presents the stress states of a confined PMMA specimen. The axial true stress σ_{axial} , equivalent stress σ_{eq} and radial confined pressure q according to the detailed analysis in Refs. [10, 16-18] are defined as follows,

$$\sigma_{\text{axial}} = \frac{F}{\pi r^2} \quad (1)$$

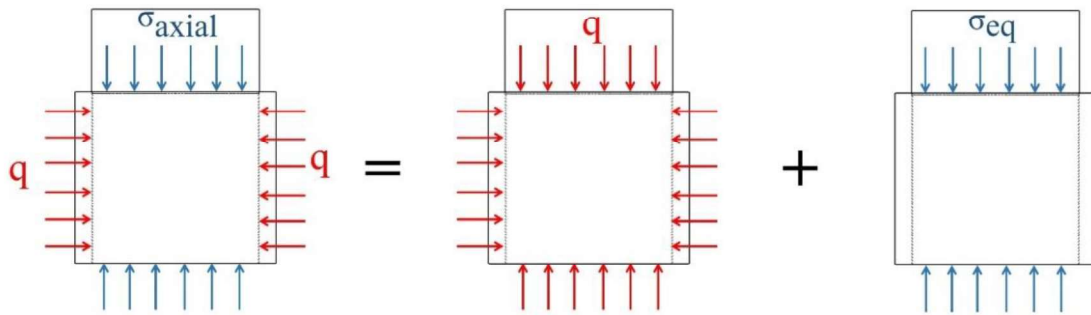
$$\sigma_{\text{eq}} = \sigma_{\text{axial}} - q \quad (2)$$

$$q = \frac{\sigma_y}{4} \left[1 - \left(1 + \frac{t}{r} \right)^{-2} + 2 \ln \left(\frac{r+t}{r} \right) \right] \quad (3)$$

where F is the applied load, σ_y , t , and r are the yield stress, wall thickness and inner radius of PMMA specimen. Here, low, medium and high confinements correspond to sleeves with 0.3 mm, 0.5 mm and 0.7 mm wall thickness. The material properties of Al sleeve were measured at the same strain rates and temperatures as the tested PMMA specimens, using cylindrical specimens with 4 mm diameter and 4 mm length.



(a)



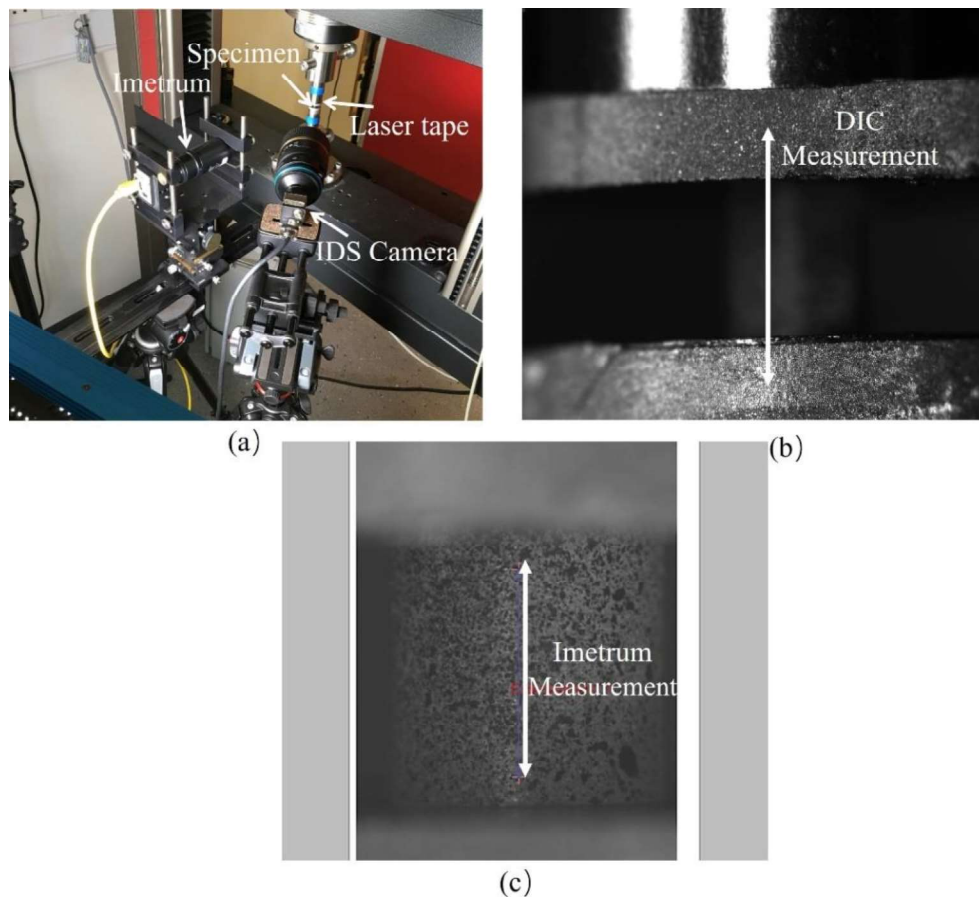
(b)

Fig.1 Specimen Assembly (a) and the schematic diagram of the stress states (b)

2.2 Experimental setup

2.2.1 Quasi-static testing

A Zwick Z50 screw driven testing machine was used to perform the compressive quasi-static tests, synchronized with an Imetrum video extensometer¹ with a frame rate of 10 fps and IDS (Image Development Systems) UEye USB 3.0 Camera² with a frame rate of 25 fps. The IDS camera comprises a CMOS sensor of resolution 2456x2054 pixels. The local cell moved at a constant speed corresponding to engineering strain rate 0.01 s^{-1} in the displacement control mode. Two laser reflective tapes were attached on the loading platens for the measurement of relative displacement of the specimen ends. A commercial DIC software LaVision Davis³ was used to obtain the engineering strain of the specimen. In addition, the specimen engineering strain is measured with the Imetrum video extensometer directly from the specimen. Hence, the engineering strain from analysis using DIC software LaVision Davis and Imetrum system can be obtained to confirm the uniform deformation of the specimen.



¹ Imetrum Limited, The Courtyard, Wraxall, Bristol, BS48 1NA, United Kingdom

² IDS Imaging Development Systems GmbH, Dimbacher Str. 6-8, 74182 Obersulm, Germany

³ LaVisionUK Ltd, 2 Minton Place Victoria Road, Bicester OX26 6QB, United Kingdom

Fig.2. Quasi-static testing setup (a) Zwick machine setup (b) Specimen from the IDS camera and (c) Real time Imetrum video extensometer

2.2.2 Medium rate testing

The medium rate compression experiments were carried out by using a hydraulic Instron machine 8854, synchronized with a Photron camera at a frame rate of 10,000 fps. The hydraulic machine is controlled by an Instron 8800 MT bi-axial digital controller, which was used to provide engineering strain rates from 1 s^{-1} - 100 s^{-1} to compress the specimen under displacement control mode.

2.2.3 Intermediate strain rate testing

The dynamic loading experimental setup is a modified bespoke 16 mm diameter split Hopkinson compression bar with 1.1 ms pulse duration capability, synchronized with a high-speed camera⁴, as can be seen in Fig.3. The apparatus comprises Ti6Al4V alloy input and output bars of 2.7 m in length and 10 mm in diameter with a 2.5 m long striker bar also made from Ti6Al4V alloy. This bespoke Hopkinson bar setup [19-22] was able to achieve strain rates between 100 s^{-1} - 1000 s^{-1} . The high-speed images recorded by using a Tamron SP60mm Macro lens mounted on the camera have a resolution of 924x748 pixels, at framing rates from 2×10^5 - 5×10^5 fps and shutter speed 2 μs . In order to evaluate the influence of environmental temperature on the response of PMMA, elevated temperature tests at 50 °C, 75 °C and 100 °C were performed by using an environmental chamber around the Hopkinson bar system. A 0.7 mm thickness neoprene rubber sheet was used as a pulse shaper and placed at the impact end of input bar to control the rise time of the incident wave signal and to achieve a constant loading rate condition. Typical incident and transmitted pulses from the bespoke Hopkinson bar apparatus are shown in Fig.4. One strain gauge bridge (Gauge 3) was attached on the output bar, and two strain gauge bridges (Gauge 1 and Gauge 2) were attached on the incident bar. With the use of a long strike bar, the incident wave and reflected wave were superimposed. It's insufficient to separate the superimposition of the incident wave and reflected wave with only one strain gauge, hence, two strain gauges were used in

⁴ Kirana camera, Specialised Imaging Ltd., LU7 9GX, Pitstone, United Kingdom

the incident bar. The details on the stress wave propagation analysis are described in Appendix B.



Fig.3 High rate experimental setup Hopkinson bar(a) and typical camera window view(b)

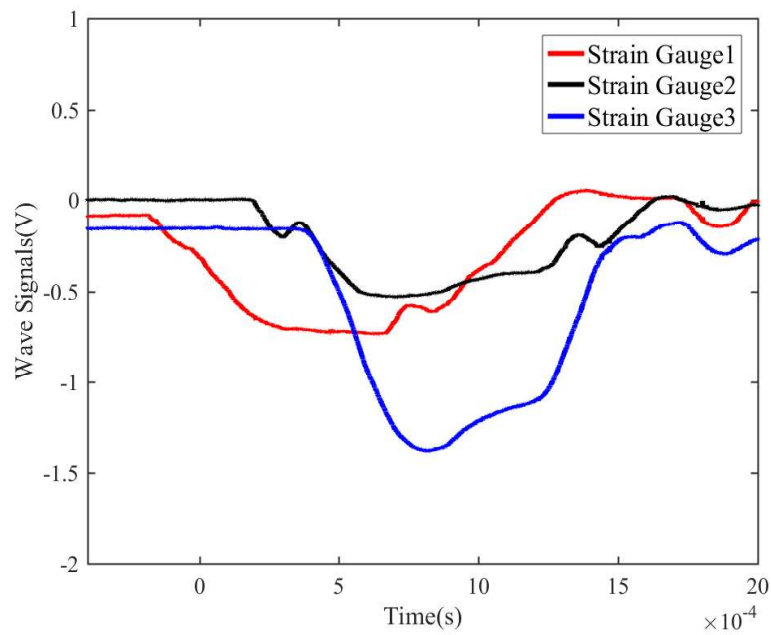


Fig.4 Typical raw signals for a confined PMMA specimen at strain rate of 270 s^{-1} at room temperature

3. Experimental Results

3.1 Quasi-static Experimental Results

The quasi-static tests were carried out at an engineering strain rate of 0.01 s^{-1} . Fig.5 shows the engineering stress-strain relationship for specimens without confinement and with 58.6 MPa lateral confinement. Both measurements from Imetrum and Laviosn Davis DIC yield identical results, indicating the uniform deformation of the specimen. The engineering stress-strain relationship of PMMA presents a response with limited strain hardening. The engineering flow stress increases from 134 MPa without confinement to 225 MPa with confinement at engineering strain 0.08, indicating the obvious pressure dependent behavior.

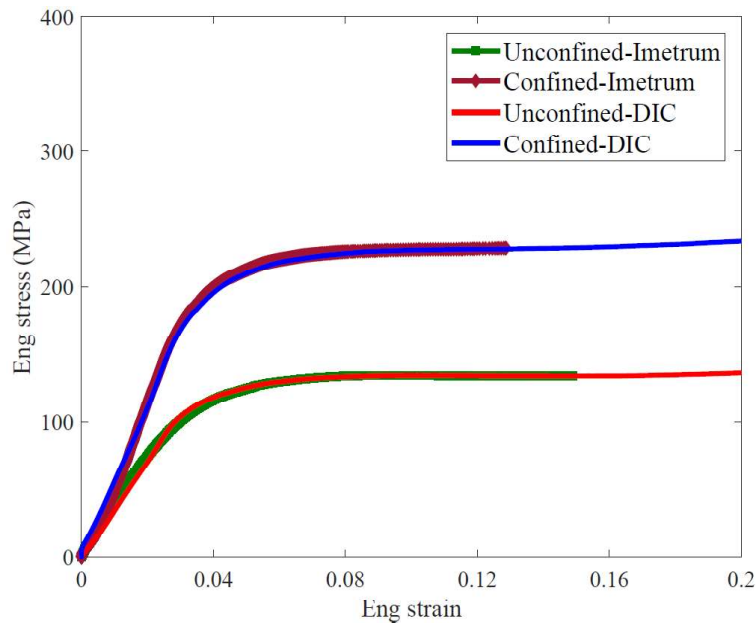


Fig.5 Engineering stress-strain relationship of confined and unconfined PMMA at engineering strain rate of 0.01 s^{-1} at room temperature

Fig.6 shows the effect of different confinements on the axial true stress as a function of axial true strain (logarithmic strain) for PMMA specimens at engineering strain rate of 0.01 s^{-1} at room temperature. Here, sleeves with 0.3mm, 0.5mm and 0.7mm wall thickness result in the confined pressure q of 37.6 MPa, 58.6 MPa, and 77.3 MPa respectively, according to Equation (3), using an average yield stress 350 MPa of the Al sleeve which was measured in separate tests at engineering strain rate of 0.01 s^{-1} and room temperature. The unconfined specimen shows the lowest flow stress at the corresponding true strains. The peak true stress values increase from 123 MPa in unconfined specimen, to 177 MPa in low confinement

specimen, 205 MPa in medium confinement specimen and eventually 236 MPa for the highest level of confinement.

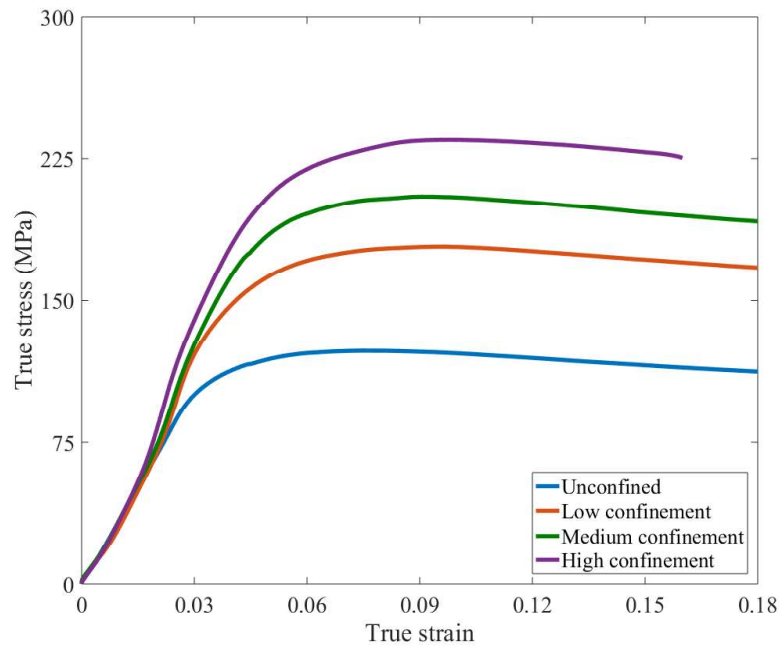


Fig.6 True stress-strain relationship of confined and unconfined PMMA at engineering strain rate of 0.01 s^{-1} at room temperature

3.2 Medium Rate Experimental Results

The medium rate tests were conducted at engineering strain rates between 1 s^{-1} - 50 s^{-1} . Fig.7 compares the true stress-strain relationship of unconfined and confined PMMA specimens at strain rate of 10 s^{-1} . Without the use of two heavy grips on the Hydraulic Instron machine, almost no oscillation can be seen in the raw stress (force) measurement shown in Fig.7. It is clear to see the effect of the confinement pressure on the peak stress. From low to high confinement, the peak stress increases from 221 MPa to 330 MPa. The peak stress as a function of lateral confining pressure at medium rates is compared in Fig.8. For three strain rates of 1 s^{-1} , 10 s^{-1} and 30 s^{-1} studied, the peak flow stress increases as the confined pressure increases. Also, it is found that the increase in peak stress for corresponding lateral confinement for these three strain rates is approximately constant, indicating the increase of strain rate dependent peak stress is independent of confined pressure.

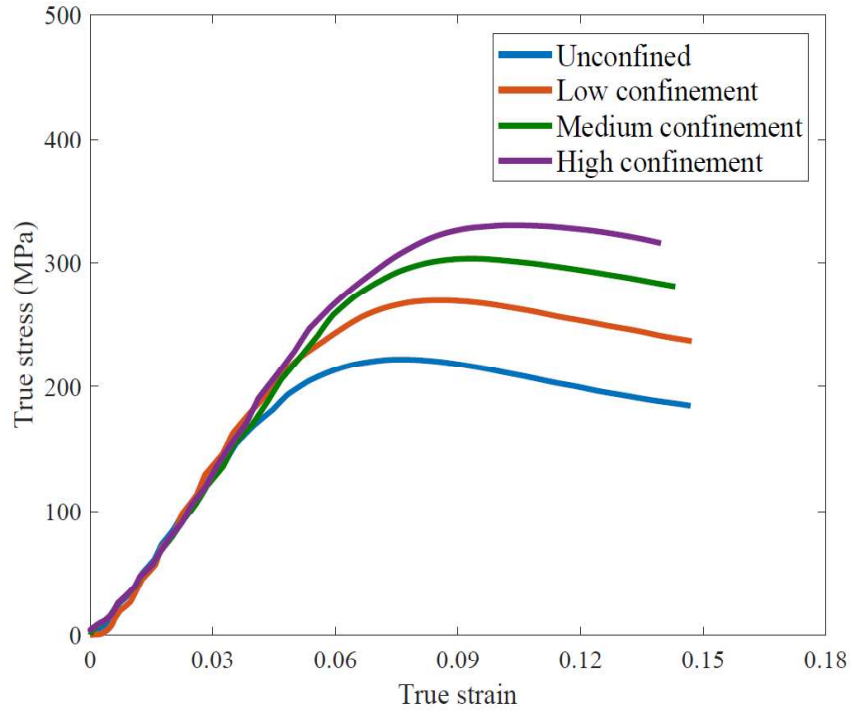


Fig.7 Comparison of the true stress-strain relationship at strain rate of 10 s^{-1} at room temperature

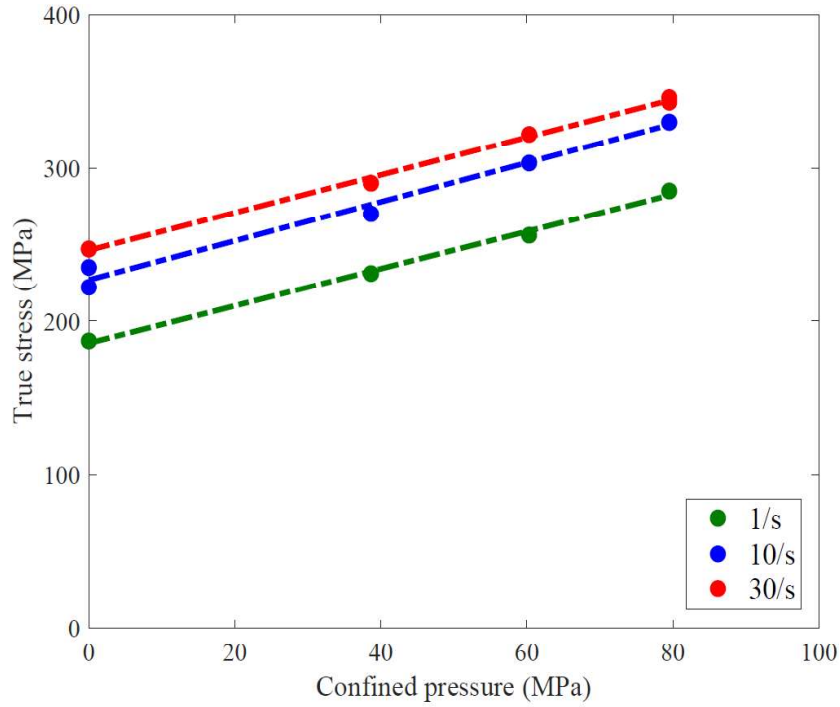


Fig.8 Peak stress as a function of lateral confinement for strain rate of 1 s^{-1} , 10 s^{-1} and 30 s^{-1} at room temperature

3.3 Intermediate Strain Rate Experimental Results

Intermediate strain rate tests were conducted at engineering strain rates from 100 s^{-1} - 1000 s^{-1} . Dynamic measurements using the Hopkinson bar require the force equilibrium at specimen ends. Fig.9 compares a typical output force and the input force. The output force extracted from the signal on the transmitted bar agrees with the input force which is measured from two strain gage signals on the incident bar. Fig.9 also shows the corresponding strain rate history, indicating the specimen deformed at an approximately constant strain rate of about 270 s^{-1} .

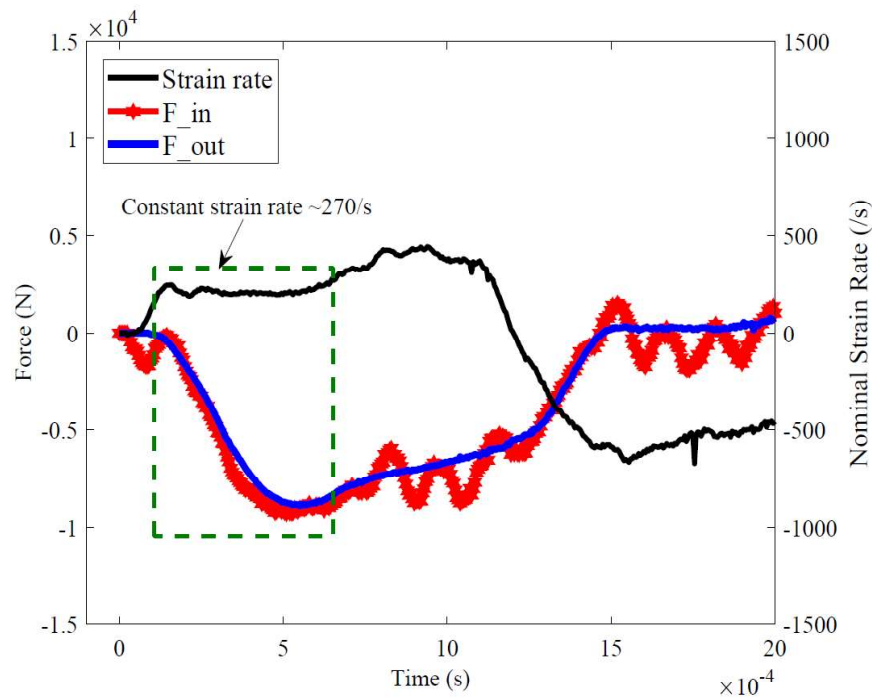


Fig.9 Typical dynamic force equilibrium conditions during Hopkinson bar experiment at 270 s^{-1} at room temperature

Regarding the strain rate effect on PMMA, Fig.10 shows the true stress-strain relationship of the unconfined specimens over a wide range of strain rates. The peak stress increases from 123 MPa at 0.01 s^{-1} , 222 MPa at 10 s^{-1} to 304 MPa at 1000 s^{-1} . The slope of the elastic (viscoelastic) part of the curve also shows apparent strain rate dependent. The PMMA presents a viscoelastic and ductile behavior at low strain rates, while the stress-strain relationship at strain rate over 270 s^{-1} exhibits a brittle behavior.

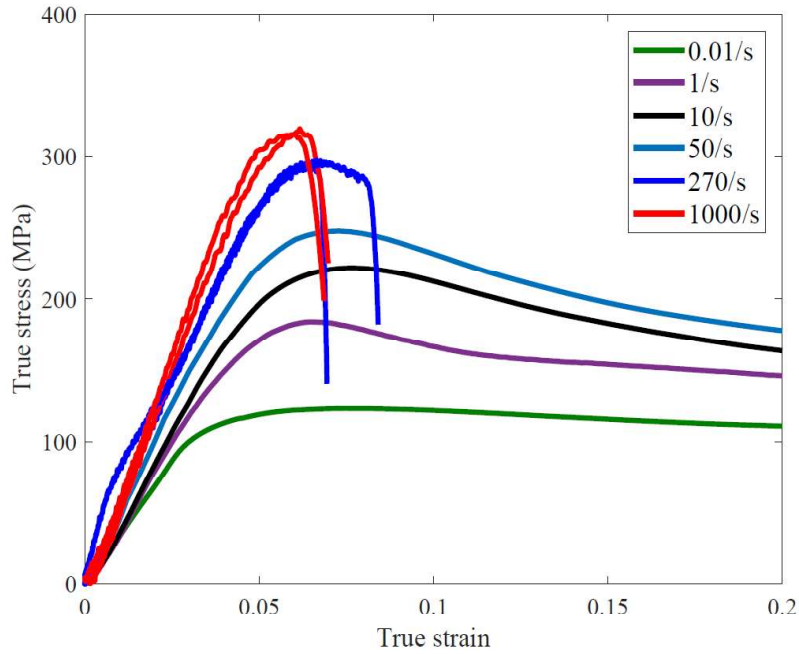


Fig.10 True stress-strain relationship for unconfined PMMA specimens without lateral confinement. Note that a noticeable strain rate sensitivity can be seen.

Typical images of the dynamic deformation process of unconfined PMMA specimen at 270 s^{-1} and room temperature are shown in Fig.11, in which the axial engineering strain is presented. The specimen at frame 59 is undergoing uniform deformation, with a slight strain (stress) concentration at the two ends. The crack initiates at the left corner marked by a white arrow, followed by the brittle fragmentation (Frame 61).

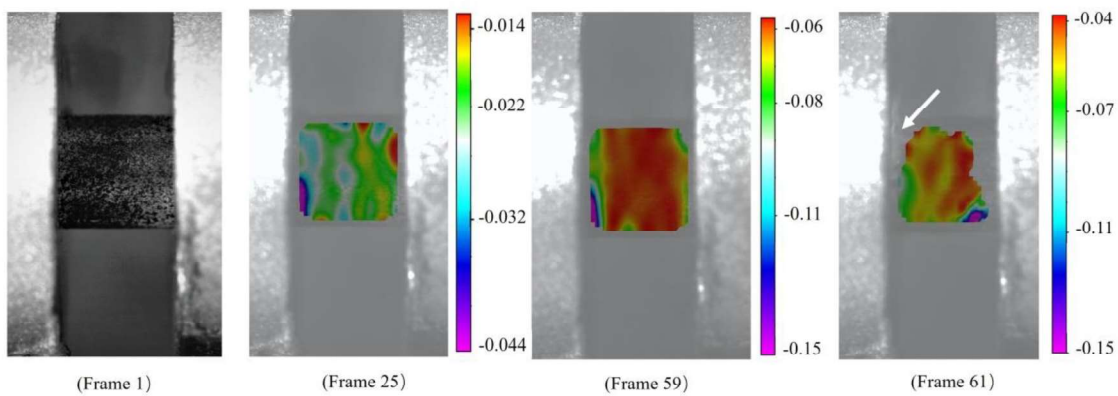


Fig.11 Dynamic deformation process of PMMA specimen with engineering strain rate of 270 s^{-1} at room temperature

Here, the peak stresses vs strain rate data of the specimens without confinement is summarized in Fig.12, together with the results in literature [7, 10, 11, 23, 24]. The increasing

trend of peak stress in the present paper is consistent with the previously published results. From the data available in the literature for PMMA, a gap exists in the data of PMMA at strain rates between 10 s^{-1} to 1000 s^{-1} , which cannot be easily achieved with conventional loading device. With the dedicated Instron machine and the bespoke built Hopkinson bar, the present data fills this gap in the strain rate dependent characterization of PMMA. Consequently, the joint effort of the results in the present paper and in literature provides a better understand of the rate dependent constitutive response of PMMA over a wide range of strain rate.

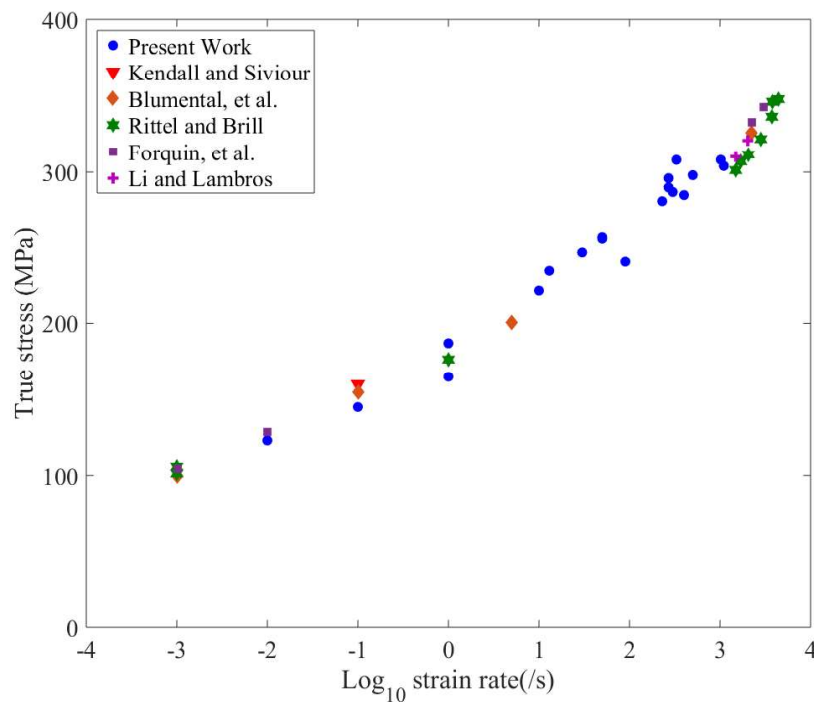


Fig. 12 Plot of peak stress vs. strain rate for unconfined PMMA specimens at room temperature

Fig.13 shows the typical true stress-strain relationship from experiments at intermediate strain rates about 300 s^{-1} for PMMA specimens without confinement and three various levels of confinement. Here, Al sleeves with 0.3mm, 0.5mm and 0.7mm wall thickness result in the dynamic confined pressure of 41.9 MPa, 65.3 MPa, and 86.1 MPa respectively. After the peak stress 296 MPa, the unconfined specimen presents strain softening, followed by a rapid load drop and fracture. When the lateral confinement is introduced, the stress-strain relationship appears to be different from the response in a dynamic uniaxial stress situation. The peak stress increased to 339 MPa for the low confinement case, however, the specimen

still fails shortly beyond the peak stress, indicating the low confinement in this instance is insufficient to suppress the brittle fragmentation in PMMA. The medium and high confinements see the peak stress increases to 358 MPa and 389 MPa respectively. In addition to the increasing peak stress with confined pressure, it is observed that the slope beyond peak shows a gradual decrease, indicating the role of lateral confinement in postponing of strain softening, similar to the results at high strain rates in Ref. [10].

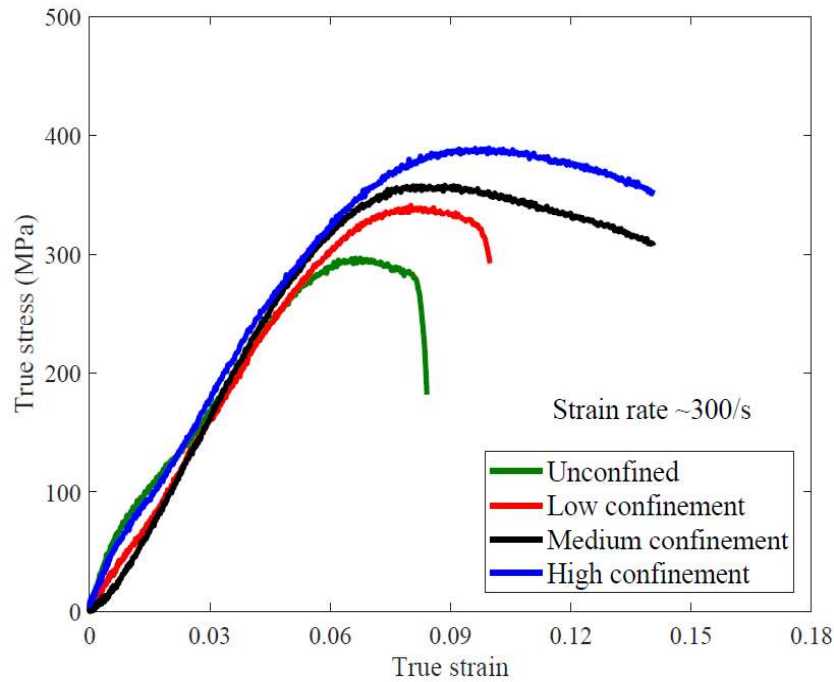
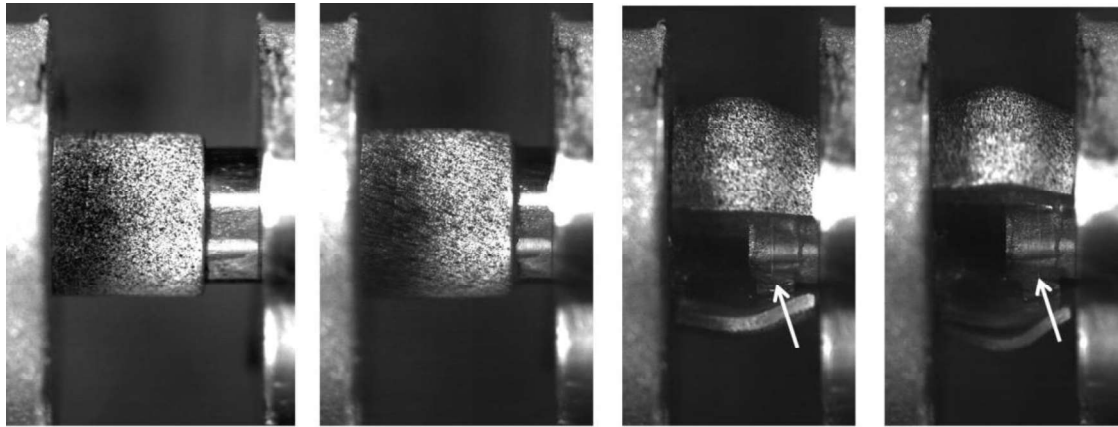


Fig.13 Typical true stress-strain relationship of PMMA under different confinement level at strain rate of about 300 s^{-1} at room temperature

Regarding high speed deformation process of the confined experiment, Fig.14 shows the deformation and fracture of PMMA specimen with medium confinement at intermediate strain rate at 270 s^{-1} at room temperature. The adapter was placed on the right side towards the incident bar, and the complete assembly is shown in Frame 1. During the experiment, the incident bar loaded the PMMA specimen confined by the Al sleeve through the adapter, thereby achieves the multi-axial loading by superposing lateral confinement upon axial compression. In Frame 166, both of the PMMA specimen and the Al sleeve fractured, and the melting PMMA filament (white arrow) can be clearly seen, indicating the high temperature characteristic associated with the dynamic failure of confined PMMA.



(Frame 1)

(Frame 80)

(Frame 166)

(Frame 177)

Fig.14 Dynamic deformation process of PMMA specimen with medium confinement at 270 s^{-1} at room temperature. The melting PMMA filament is marked by a white arrow, indicating the high temperature characteristic.

The unconfined specimen tested at intermediate strain rate was fragmented completely, which is similar to other traditional brittle glass materials. With lateral confinement, the brittle feature of PMMA specimen can be retained by the plastically deformed Al sleeve. Fig.15 shows the typical recovered conical shape of confined PMMA specimen (gold coated for further microstructural analysis), together with the Ti6Al4V adapter and the fractured Al sleeve. The conical plug is a truncated cone, the top of which was loaded by the adapter dynamically, while the base of the cone formed inside the PMMA specimen. The propensity to crack and fragment appears to be suppressed by the confinement pressure, and the specimen exhibits ductile failure characteristic.

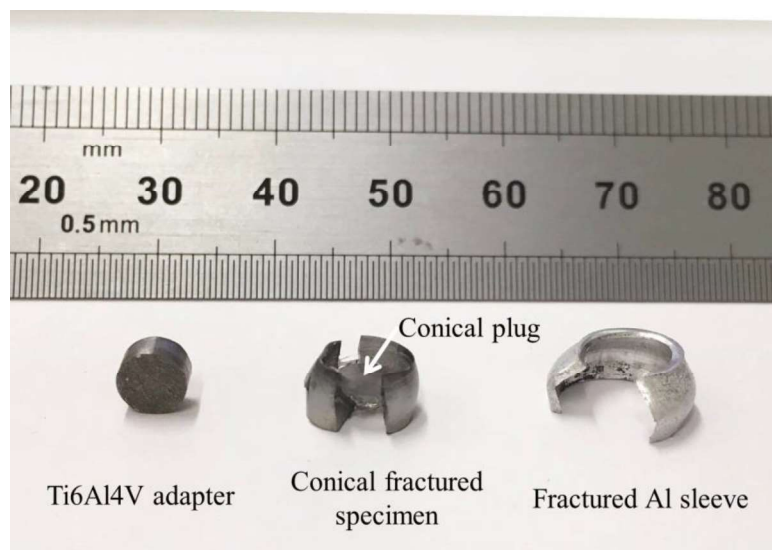


Fig.15 Recovered fractured confined PMMA specimen at strain rate of 270 s^{-1} at room temperature

The variation of the peak stress as a function of the confined pressure is shown in Fig.16, for PMMA specimens without confinement and with different confinements tested at intermediate strain rates. Apparently, as the lateral confined pressure increases from 0 to 86.13 MPa, the peak stress increases monotonically from 296 MPa to approximately 406 MPa.

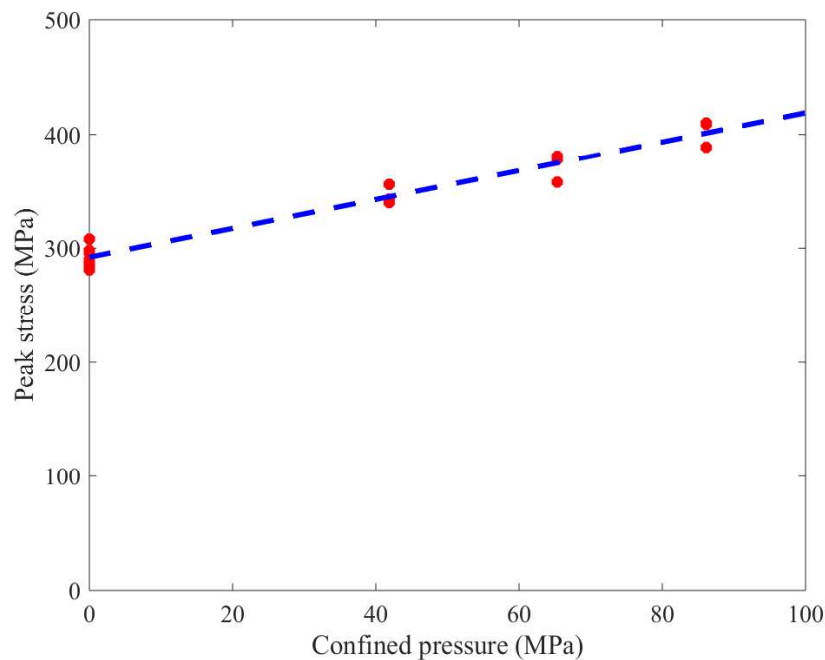


Fig. 16 Variation of peak stress of PMMA with confinement at strain rates of $200\text{-}500 \text{ s}^{-1}$

3.3 Intermediate Strain Rate Results at Elevated Temperatures

Fig.17 shows the typical true stress-strain relationship of PMMA specimens with low confinement at intermediate strain rates at four temperatures. Beyond the peak stress 339 MPa, the specimen with low confinement fails rapidly with fragmentation, thus the low confinement cannot delay the brittle failure of PMMA. However, when the temperature increases to 50°C , the specimen presents ductile behaviour and similarly for the confined tests at 75°C and 100°C . Consequently, the higher temperatures are able to suppress the brittle fragmentation of PMMA at low confinement pressures 41.9 MPa at 50°C and 75°C and 37.6 MPa at 100°C .

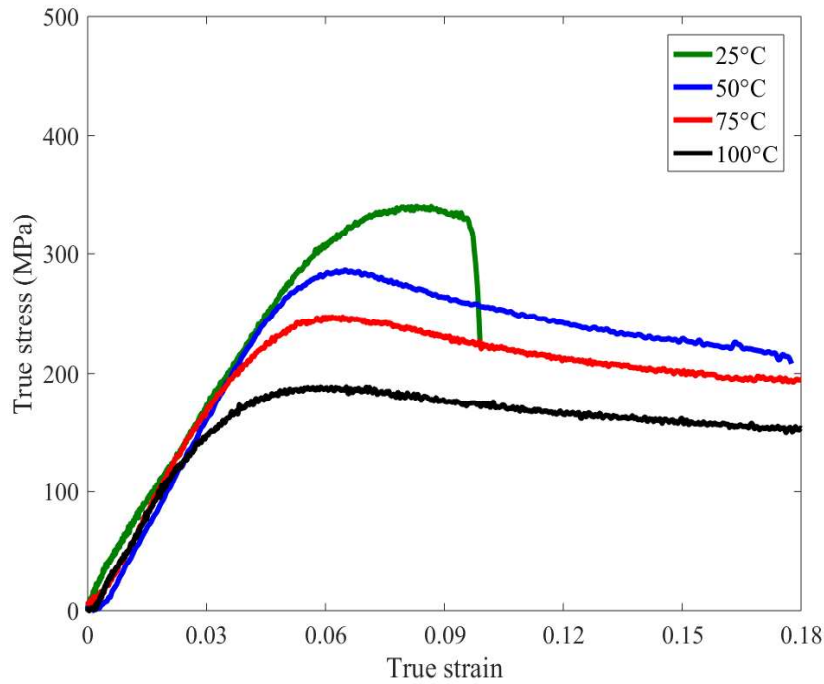


Fig.17 Typical true stress-strain relationship of PMMA under low confinement level at different temperatures at intermediate strain rates

Fig.18 shows a plot of compressive peak stress versus temperature for PMMA without confinement and three different levels of confinement. As the temperature increases from 25 °C to 100 °C, the unconfined peak stress decreases monotonically from about 292 MPa to 145 MPa, whereas the peak stress with high confinement decreases monotonically from 409 MPa to 253 MPa. A similar descending trend can be observed for low and medium confinement cases. The increase of peak stress from the unconfined situation to the high confinement indicates the pressure effect for all temperature conditions.

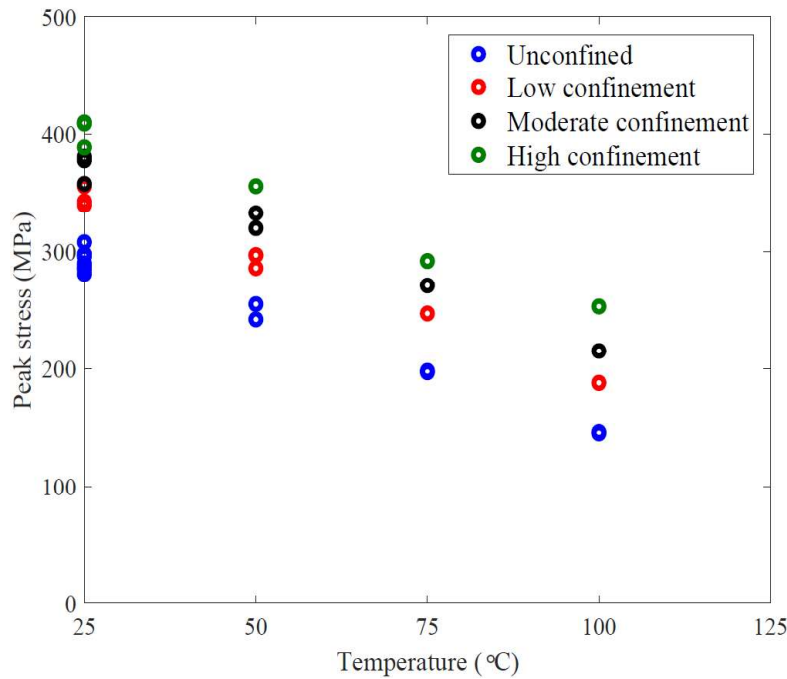


Fig.18 Effect of temperature and confinement on the peak stress of PMMA at intermediate strain rates

3.4 Microstructural Characterization

The fracture morphology of fractured specimens tested at intermediate strain rates was analysed using a Carl Zeiss Evo LS15 VP-Scanning Electron Microscope. Prior to SEM characterization, the PMMA specimens were carefully placed onto sample mounts with double-sided conductive carbon tape and coated with gold to reduce charging, using a Quorum Technologies SC7620 mini sputter coater. The specimen without lateral confinement at room temperature was completely fragmented, and a typical micrograph of the fracture morphology of brittle fractured specimen is presented in Fig.19a and Fig.19b, the latter being higher magnification for the square area in Fig.19a, and highlights a rough hackle landscape feature.

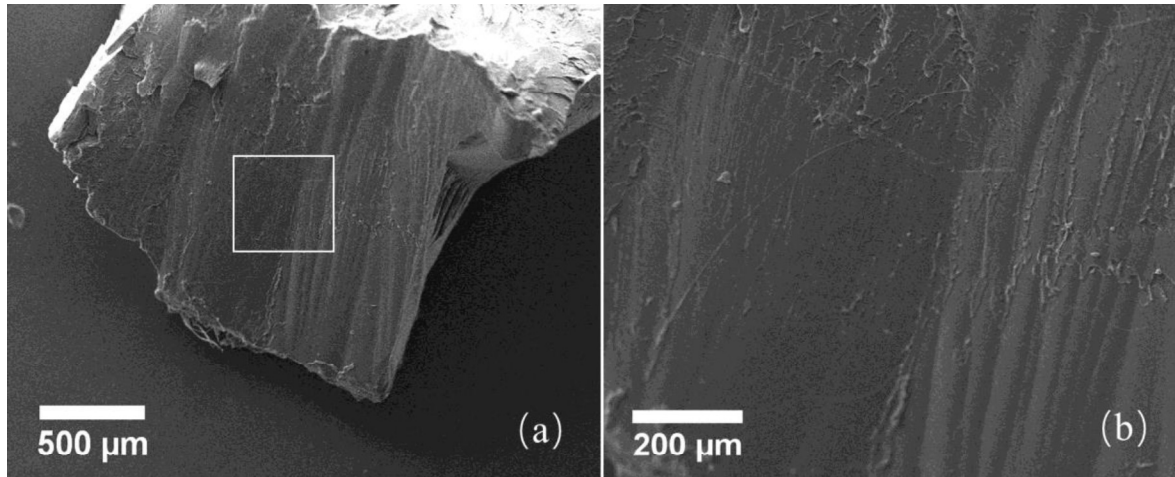


Fig.19 Fracture surface electron images taken from a radial fragment in an unconfined specimen at room temperature

Fig.20 shows the fracture morphology of the specimen with low confinement at room temperature at intermediate strain rate, the propensity to crack growth appears to be suppressed by the confined pressure, and the fragmented specimen size is apparently larger than that in an unconfined specimen in Fig.19. A similar rough landscape can be seen in Fig.20b (closer view of the square area in Fig.20a), indicating the brittle failure characteristic of PMMA.

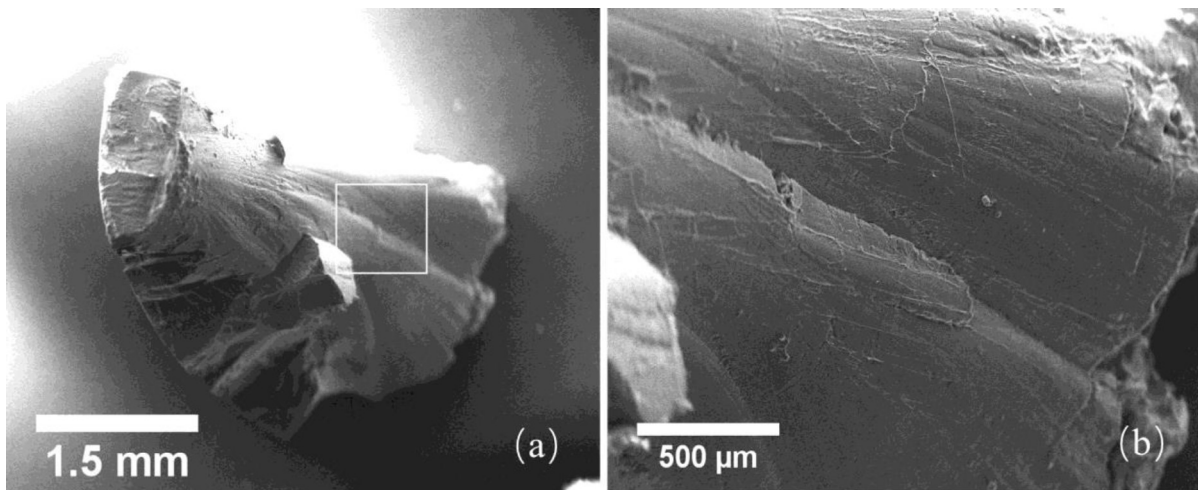


Fig.20 Fracture morphology of PMMA specimen with low confinement at intermediate strain rate room temperature

Next, the conical fracture surface of a PMMA specimen with medium confinement at room temperature is examined and compared to the above fracture morphology for specimens without confinement and low confinement. Fig.21 shows the typical conical plug from a specimen with medium confinement tested at intermediate strain rate at room temperature. The envelope of the cone is composed of elongated dimples (white arrow) in Fig.21b, and a closer view clearly indicates melting has occurred in Fig.21c. These elongated dimples and the material thermal softening indicate the highly localized shear failure mode in PMMA at intermediate strain rate with medium lateral confinement. The melting PMMA filament observed in high-speed images in Fig.14 and the present fracture surface micrograph indicate the conical plug is a result of adiabatic shear banding.

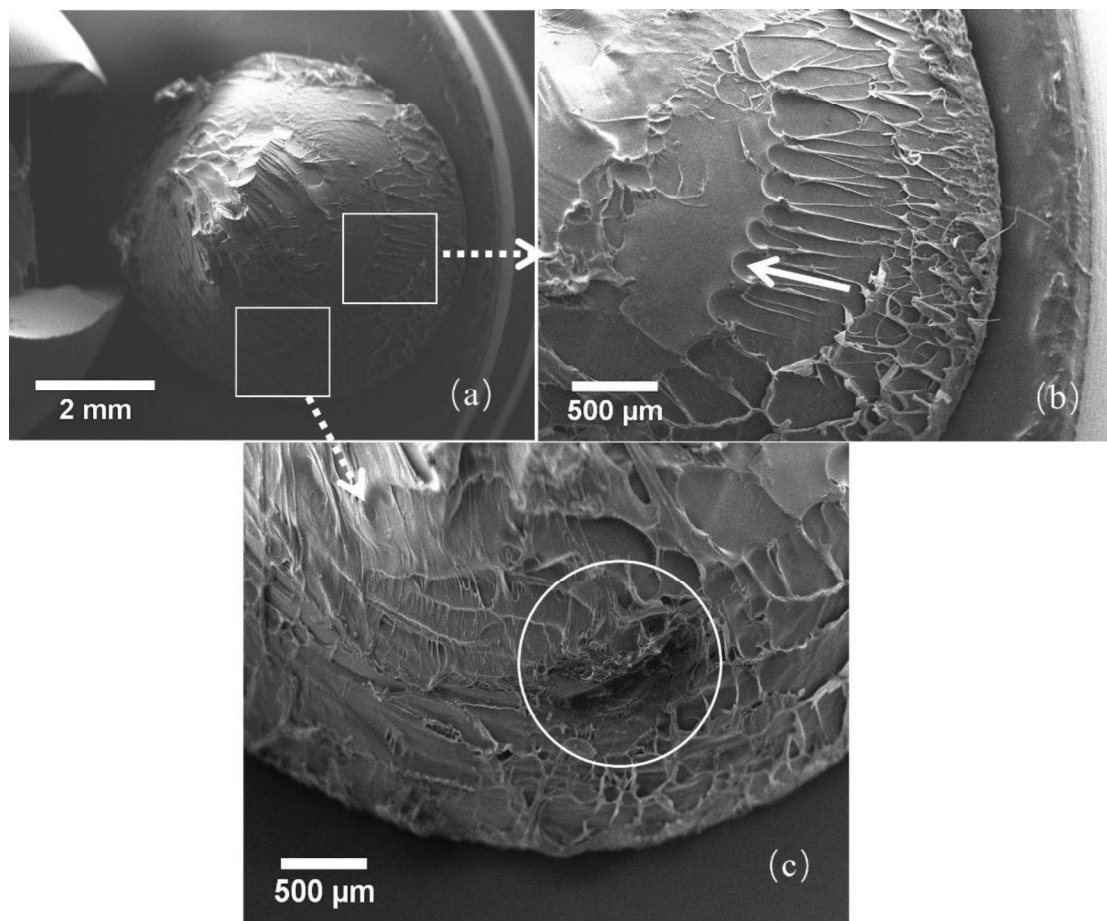


Fig.21 Representative fracture morphology of specimens with medium confinement at intermediate strain rate at room temperature.

Fig.22 presents the fracture surface of PMMA specimen with low confinement tested at intermediate strain rate of 300 s^{-1} at $50 \text{ }^{\circ}\text{C}$. The cup surface and the cone surface are shown in Fig.22a and Fig.22b, respectively. Several almost parallel PMMA filaments (white arrows) aligned to the shear direction and distributed on the cup fracture surface, and are associated with high temperature rise during the deformation of PMMA. Likewise, the melting signs marked by the white circles in Fig.22b also indicate a noticeable thermal softening mechanism in the highly localized cone fracture surface. Compared to the rough landscape in PMMA specimen which failed in a brittle manner with low confinement tested at intermediate strain rate at room temperature shown in Fig.20, the PMMA filaments and melting signs clearly indicate the adiabatic shear failure mode in PMMA specimen with low confinement tested at intermediate strain rate at $50 \text{ }^{\circ}\text{C}$. Therefore, in addition to applying higher confinement, the higher temperature is also able to induce the brittle to ductile transition of PMMA.

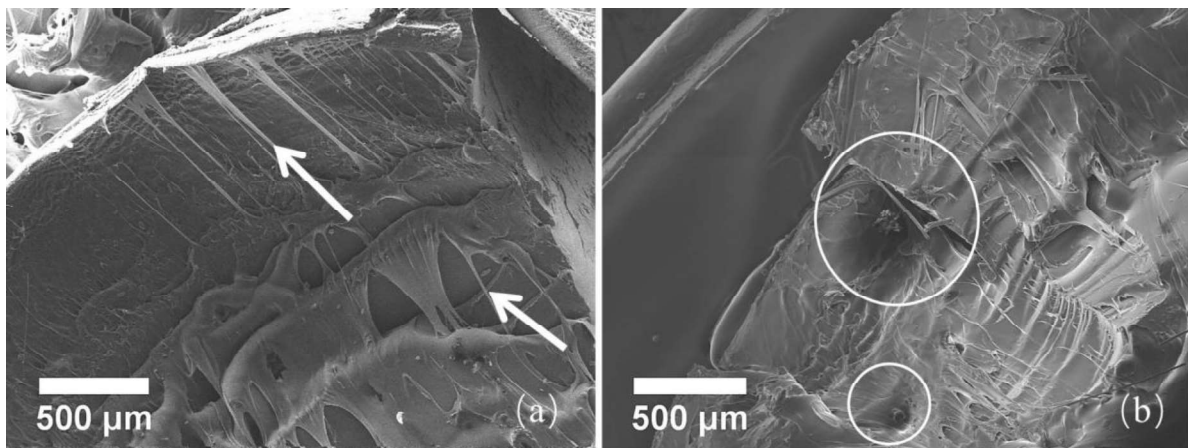


Fig.22 Fracture morphology of specimen with low confinement at intermediate strain rate at $50 \text{ }^{\circ}\text{C}$.

4. Constitutive Modelling

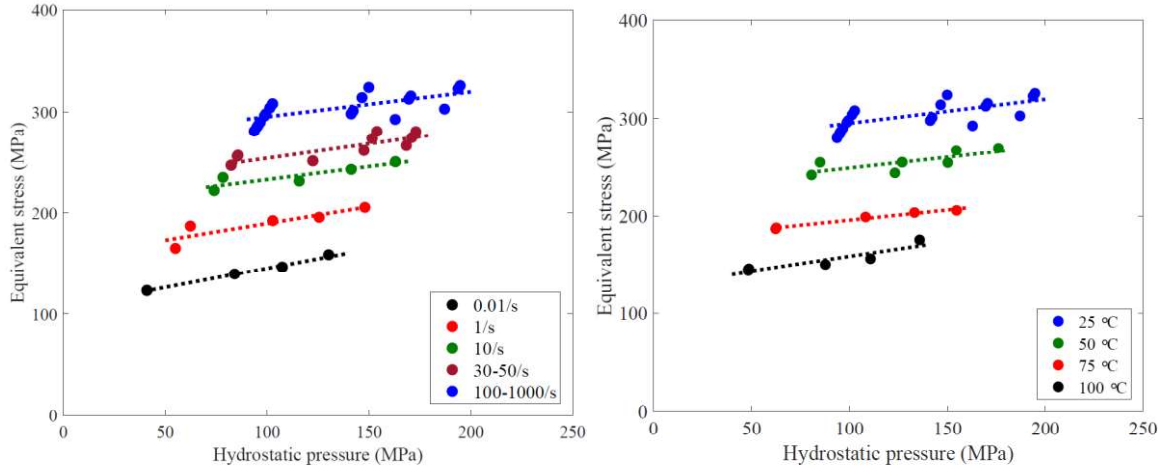
4.1 Pressure Sensitivity

The Drucker-Prager (DP) model, initially proposed by Drucker and Prager [25], has been widely used to describe pressure sensitivity of the deformation of soils in the last several decades. Variants in the DP model can be also applied to other pressure dependent materials like polymers. Here, the DP pressure criterion [26] is employed to describe the pressure sensitivity of confined PMMA, which is described as follows:

$$\sigma_{eq} + \alpha p - \left(1 - \frac{1}{3}\alpha\right) \sigma_c = 0 \quad (4)$$

$$p = \frac{1}{3}(\sigma_{axial} + 2q) \quad (5)$$

where σ_c is true yield stress under uniaxial compression, p is the hydrostatic pressure. α is the pressure sensitivity coefficient. This DP model provides a potential approach to describe the relationship between the equivalent stress of PMMA with different levels of confinement and strain rates. In order to determine the pressure sensitivity, Fig.23a presents the equivalent stress and pressure data at strain rates from 0.01 s^{-1} to 1000 s^{-1} at room temperature, together with the data at intermediate strain rates at different temperatures in Fig.23b. The first visual observation of Fig.23 shows the fitted lines are almost parallel, indicating the moderate effect from the strain rate and temperature dependence on the pressure sensitivity description. The average fitted parameter is $\alpha=0.274$ in DP pressure model. The pressure sensitivity is not apparently strain rate and temperature dependent, consequently, pressure, strain rate and temperature effects can be decoupled and addressed separately, by using a simple constitutive relationship. Fig.23 also shows that the intermediate and high rate data are above the low rate data, whereas the high temperature data are below the room temperature data, indicating the significant temperature and strain rate dependent response of PMMA. However, the increasing lateral confinement gradually increases the stress values, compared to the observed roles of temperature and strain rate, which have a greater influence on the flow stress values of PMMA.



(a) Effect of strain rate at 25 °C (b) Effect of temperature at 100-1000 s⁻¹

Fig.23 Equivalent stress as a function of hydrostatic pressure for unconfined and confined PMMA

4.2 Strain rate and Temperature Sensitivity

The strain rate and temperature dependence of peak stress of unconfined PMMA is analysed, by using a power law rate dependent model and a linear thermal softening model, which is defined as:

$$\sigma_c = \sigma_{ref} \left(\frac{\dot{\epsilon}}{\dot{\epsilon}_{ref}} \right)^n [1 - m(T - T_r)] \quad (6)$$

Here, σ_{ref} is the peak equivalent stress at reference strain rate $\dot{\epsilon}_{ref}$ 0.01 s⁻¹, $\dot{\epsilon}$ is the strain rate, T is the current temperature, T_r is the reference temperature 25 °C, n and m are the parameters describing the strain rate sensitivity and thermal softening. Fig.24 shows the peak equivalent stress of PMMA at strain rates from 0.01-1000 s⁻¹ without lateral confinement at room temperature. The fitted model is $\sigma_c = 123 \left(\frac{\dot{\epsilon}}{0.01} \right)^{0.0826}$. The simple model is capable to describe the strain rate dependence on the experimental stress.

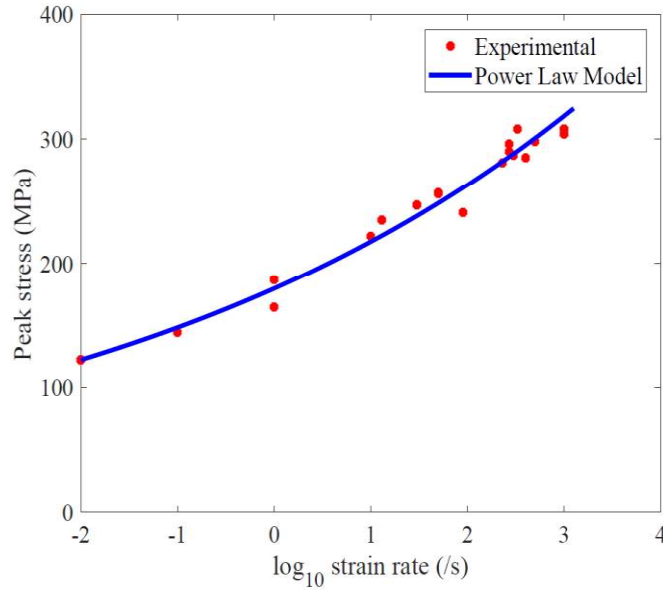


Fig.24 Strain rate dependence of the peak stress for unconfined PMMA at room temperature

Considering the temperature sensitivity, Fig.25 shows the results of peak stress of PMMA specimens at intermediate strain rates without confinement under different temperature conditions. The peak stress is found to decrease linearly with the increasing temperature from 25 °C to 100 °C. Here, the temperature dependent parameter m in Equation (6) is used to describe the thermal (softening) effect, with the fitted value $m=0.0068$. Note that the power law rate dependent model and thermal softening model in the present paper show the simplest phenomenological nature of PMMA, while more sophisticated constitutive relationship can be found in the previous pioneering work of Richeton et al. [27].

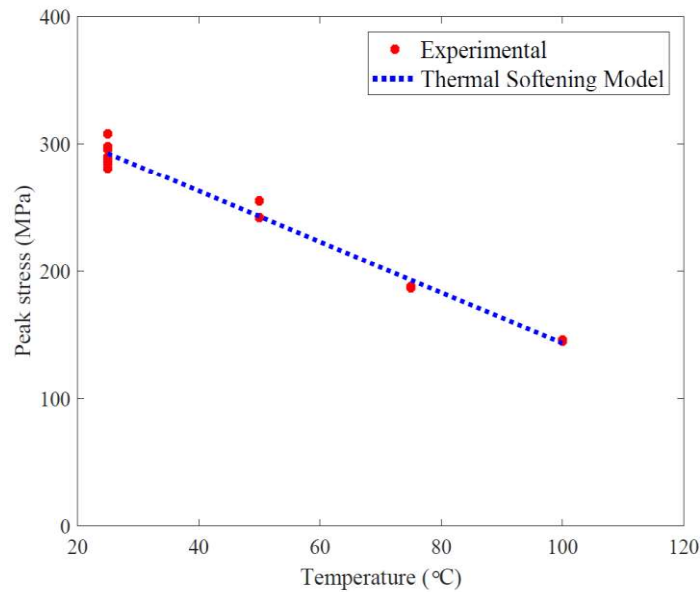


Fig.25 Effect of temperature on the peak stress of unconfined PMMA at intermediate strain rates

Finally, combining the strain rate, temperature and pressure sensitivity results for PMMA, the final simple constitutive law in Equation (4) can be expressed as follows:

$$\sigma_{eq}^{peak} + 0.274p = 111.8 \left(\frac{\dot{\epsilon}}{0.01} \right)^{0.0826} [1 - 0.0068(T - 25)] \quad (7)$$

The equivalent stress and strain can be transferred to shear stress and strain by assuming

$\tau_{flow} = \frac{1}{2} \sigma_{eq}$ and $\dot{\epsilon} = \frac{1}{2} \dot{\gamma}$ according to Refs. [10, 18, 28], thus Equation (7) reduces to

$$\tau_{flow}^{peak} = 55.9 \left(\frac{\dot{\gamma}}{0.02} \right)^{0.0826} [1 - 0.0068(T - 25)] - 0.137p \quad (8)$$

4.3 Brittle to Ductile Failure Transition

The applied confined pressure increases the peak stress, while the slope in the stress-strain relationship beyond peak shows a gradual decrease at intermediate strain rates, indicating the role of pressure on the strain softening evolution. PMMA without confinement fails in brittle fragmentation. However, with the introduction of lateral confinement, the failure mode exhibits adiabatic shear localization under medium lateral confinement pressure at room temperature and elevated temperatures. The melting PMMA filament observed in high speed images, together with the microstructural analysis, confirms the adiabatic shear banding failure in confined PMMA at intermediate strain rates. Here, the shear stress and hydrostatic pressure of confined specimens with adiabatic shear failure at intermediate strain rates are shown in Fig.26, in order to better understand the transition between brittle and ductile shear failure. The DP model description in Equation (8) is added into for a comparison of experimental results for a corresponding shear strain rate of 600 s^{-1} at $25 \text{ }^{\circ}\text{C}$, $50 \text{ }^{\circ}\text{C}$ and $75 \text{ }^{\circ}\text{C}$. It is found that the proposed temperature and strain rate dependent DP model data is consistent with the experimental data at three temperatures. Below 150 MPa, the material fails in a brittle mode at intermediate strain rates at room temperature. However, this threshold is not constant. When the temperature increases to $50 \text{ }^{\circ}\text{C}$ and $75 \text{ }^{\circ}\text{C}$, the critical pressures decrease to 123 MPa and 108 MPa, indicating the temperature effect also plays an important role in suppressing the brittle failure.

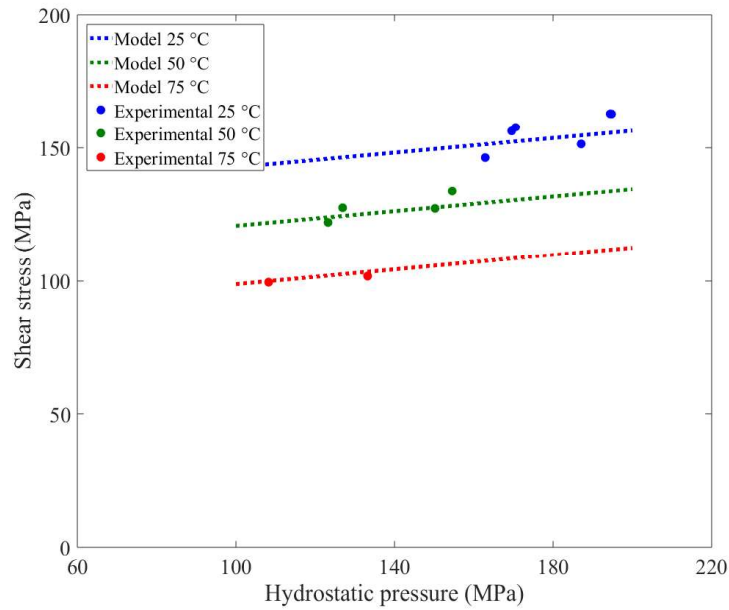


Fig.26 Peak shear stress as a function of hydrostatic pressure for specimens with adiabatic shear failure at intermediate shear strain rates about 600 s^{-1}

5. Discussion

The present paper studies the compressive response and failure behaviour of PMMA without confinement and with various levels of lateral confinement from quasi-static, medium rates and intermediate strain rates loading. In addition to rate dependent characterization, the temperature dependent response of PMMA at intermediate strain rates is also investigated. The mechanical behaviour of PMMA has been extensively reported across several strain rate regions in literature, except the strain rate between 10 s^{-1} - 1000 s^{-1} , which posed a challenge for the conventional testing equipment. However, PMMA windshields of aircraft and high speed train experience this strain rate region under ice and bird strikes. Studies to provide mechanical characterization of PMMA at these intermediate strain rates would benefit the impact resistant engineering structural design. The present paper reports the behaviour of unconfined and confined PMMA over a wide range of strain rates (and temperatures) and fill this gap at the strain rate level of 10 s^{-1} - 1000 s^{-1} by employing a specialised hydraulic Instron machine, and bespoke long Hopkinson bars with pulse shaper technique to control the rise time of the incident pulse and to achieve a constant loading rate condition. The long duration stress wave generated by a 2.5 m length striker bar successfully loaded the specimen to fracture at intermediate strain rates. The material presents noticeable strain rate, pressure

and temperature and sensitivities. The peak stress increases with the increase of strain rate, in agreement with the previous results in literature. For the confined pressure effects, the peak stress tends to increase linearly with the increasing confinement pressure. In contrast, the peak stress decreases at higher temperatures. It is found that the equivalent stress in confined PMMA is only slightly higher than that in PMMA without confinement, in agreement with the finding reported by Forquin et al. [11]; however, it is much more sensitive to strain rate and temperature.

Considering the failure mode transition at intermediate strain rates, the PMMA specimens without confinement and low confinement failed in a brittle manner with dynamic fragmentation at room temperature. However, the failure mode changes to ductile shear failure under medium confinement and high confinement condition, indicating that the higher pressures applied in the PMMA can delay and suppress the brittle fragmentation and result in shear localization. In addition to increasing the peak stress by the confinements at room temperature, observations of the true stress-strain relationship show a gradual decrease of slope in stress-strain relationship beyond peak at intermediate strain rates at room temperature, indicating that the pressure affects the strain softening evolution. With the assistance of the high-speed camera, the dynamic deformation of confined PMMA was recorded, clearly showing the melting PMMA filament in the shear localization zone associated with high adiabatic temperature. The recovered failed confined PMMA specimen exhibits a conical fracture shape. The microstructure characterization in Fig.21 presents that PMMA with medium confinement fails by adiabatic shear with shear dimples and the apparent melting signs, which is a typical characteristic of the dynamic ductile failure mode and similar to dynamic shear failure of metals [29]. This is quite different from the brittle rough hackle landscape microstructures in PMMA without confinement and with low confinement in Fig.19 and Fig.20. Forquin et al. [11] observed brittle behaviour for both unconfined and confined PMMA at high strain rates. The results presented here, however, indicating that the PMMA with medium confinement fails by shear localization at intermediate strain rates at room temperature, in line with the failure modes of PMMA reported by Winter et al. [8] and Rittel et al. [10]. It is interesting to note that, although the low confinement is insufficient to suppress the brittle failure of PMMA, when the temperature increases to 50 °C, the specimen with low confinement also presents ductile shear failure. A number of PMMA filaments aligned with the shear direction and distributed on the cup fracture surface, together with the melting signs in the cone fracture surface, clearly indicate the adiabatic shear failure mode in PMMA specimen with low confinement

tested at intermediate strain rate at 50 °C. Hence, the higher temperature can also induce the brittle to ductile transition of PMMA, At 100 °C close to the glass transition region, all PMMA specimens present a rubbery response. This temperature region is generally out of the maximum service temperature of windshield, the rubbery behaviour is not the focus in the present paper and consequently not discussed further here.

The DP model is used to describe the strain rate, pressure and temperature sensitivity of the PMMA across a range of strain rates. Observations of the peak equivalent stress vs hydrostatic pressure show that the pressure sensitivity coefficient is not apparently affected by strain rate and temperature, in agreement with the reports in literature. The increasing lateral confinement only gradually increases the stress values, while it can be seen that temperature and strain rate play a more significant role in the behaviour of PMMA. Analysis of the strain rate dependence of peak equivalent stress of PMMA shows a rate dependent model based on power law is capable of describing the strain rate dependence on the experimental data. Considering the peak stress decreases linearly with increasing temperature, a simple thermal softening parameter is used to describe the temperature dependent behaviour of PMMA. It is found that the proposed temperature and strain rate dependent DP model predicts accurately the experimental data at three temperatures. Note that the present power law rate dependent and thermal softening models show the simplest phenomenological nature. More sophisticated constitutive relationship developed previously can be found in Refs. [27, 30].

PMMA used as windshield components [31-35] is designed to resist external impact events such as bird strike. Investigation on the dynamic mechanical behaviour of PMMA is critical to ensure the passenger safety and windshield structural integrity. The intermediate strain rate characterization is important for engineering design and the main concern in the present paper. Based on the service condition of PMMA in engineering applications, the temperature dependent response of PMMA is also studied. The comparison between the unconfined and confined PMMA indicates a potential strengthened technique by applying the lateral confinement or pressure to PMMA, in order to suppress the brittle fragmentation. The experimental condition in the present paper can be further extended to wider temperature regions below room temperature. In addition to the compression response, it is also important to understand the confined tensile behaviour of PMMA. Future work will aim at studying and comparing the confined compressive and tensile response of PMMA across a wide range of

strain rates (and temperatures), to systematically reveal the strain rate, pressure and temperature dependent behaviour of PMMA.

6. Conclusions

This paper investigates the compressive response of unconfined and confined PMM at quasi-static 0.01 s^{-1} , medium rate $1\text{-}100 \text{ s}^{-1}$, and intermediate strain rates $100\text{-}1000 \text{ s}^{-1}$ at room temperature $25 \text{ }^{\circ}\text{C}$, elevated temperatures $50 \text{ }^{\circ}\text{C}$, $75 \text{ }^{\circ}\text{C}$ and $100 \text{ }^{\circ}\text{C}$. The experimental measurements and the proposed model potentially can be used for the study of impact resistant applications, e.g. windshield applications. The main outcomes are summarized as follows:

- A broad range of strain rates has been applied to the unconfined and confined PMMA specimens on various loading platforms synchronized with high speed cameras, thus bridging the gaps existing in the rate dependent characterization of PMMA in the literature.
- The PMMA already exhibits brittle behavior in the intermediate strain rate region.
- A transition to ductile failure mode transition with adiabatic shear localization occurs with the introduction of medium confinement at intermediate strain rates, which can be observed from melting flow PMMA filaments in real time image recording and from SEM fractography analysis.
- A series of experiments over a range of elevated temperatures shows that the brittle to ductile transition can also occur in the low confinement condition at high temperature.
- At high temperature close to the glass transition, all unconfined and confined PMMA specimens present ductile and rubbery behavior.
- It is also found that the strain rate and temperature have more influence on the peak stress of PMMA than the pressure effect.
- The temperature and strain rate effects on the pressure sensitivity of PMMA are found to be decoupled. Thus, a simple DP model is proposed to describe the strain rate, pressure and temperature dependent response of PMMA.

Acknowledgements

The authors thank Mr. P. Tantrum, Mr. S. Carter, Mr. J. Fullerton, Mrs. K. Bamford, Dr. K. Dragnevski and Dr. M. Tkaczyk for their assistance. Mrs. N. Stivi and Mr. Y. Rozitski are appreciated for the in person introduction of the confinement technique proposed by Prof. D. Rittel at the Technion-Israel Institute of Technology. The discussion on thermomechanical response of polymers with Prof. C. Siviour is appreciated. Likewise, the finding of dynamic (adiabatic) shear failure of PMMA pointed out by Dr. R. Winter and Prof. J. Field in Cavendish Laboratory and by Prof. D. Rittel at the Technion is acknowledged.

Appendix A

Numerical simulations were performed using the commercial finite element code ABAQUS to evaluate the influence of friction between the PMMA specimen and the Al sleeve on the axial engineering stress. The specimen was modelled as axisymmetric to reduce the computational cost. The specimen and the sleeve are meshed using 4-node quadrilateral elements (reduced integration element CAX4R) of size equal to $0.1 \times 0.1 \text{ mm}^2$ and default hourglass control. The friction between the PMMA specimen and the Al sleeve was modelled using tangential contact with Coloumb friction coefficient μ equal to 0.03. This is a typical value included between the friction coefficients 0.02-0.04 examined by Davies and Hunter [36], Gorham et al. [37], Walley and Field et al. [38] for a large number of polymers when suitable lubrication and great care to reduce friction was used, and close to the recent finding reported by Durand et al. [39]. The velocity boundary conditions applied correspond to a nominal strain rate of 400 /s. The PMMA and Al sleeve are assumed to obey the Von Mises criterion with the experimentally measured stress–strain relationship as input data for the finite element analysis.

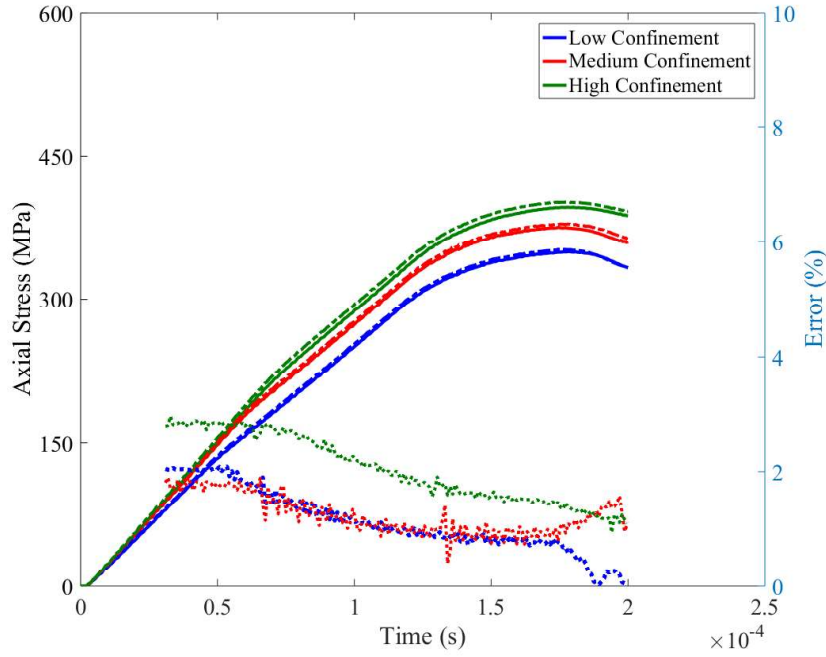


Fig.A1 Influence of friction between the PMMA specimen and the Al sleeve on the axial stress and relative error data. Different colors represent different confinements. The solid line refers to the axial stress with perfect lubrication ($\mu = 0$), while the dashed line shows the axial stress with lubricated friction ($\mu = 0.03$).

In Fig.A1, the solid line and dashed line represent the axial stress measured when assuming perfect lubrication and lubricated friction respectively. It is evident that the axial stress increases with higher lateral confinements. The axial stress obtained considering friction is slightly higher than that obtained considering perfect lubrication for all confinements. The quantitative comparison of the axial stress with perfect lubrication and with lubricated friction shows that the errors are in the range of 0-2%. Consequently, the effect friction between the lubricated PMMA specimen and Al sleeve is not considered in the present paper.

Appendix B

The incident and reflected stress waves normally do not superimpose during tests conducted using the short projectile. The strain and stress histories can be obtained via the classical spilt hopkinson bar analysis [40]. When the long striker is used, the incident and reflected waves superimpose, as can be seen from the stress wave propagation in Fig.B1. Therefore, it is not

possible to distinguish the incident and the reflected waves from only one strain gauge measurement on the incident bar.

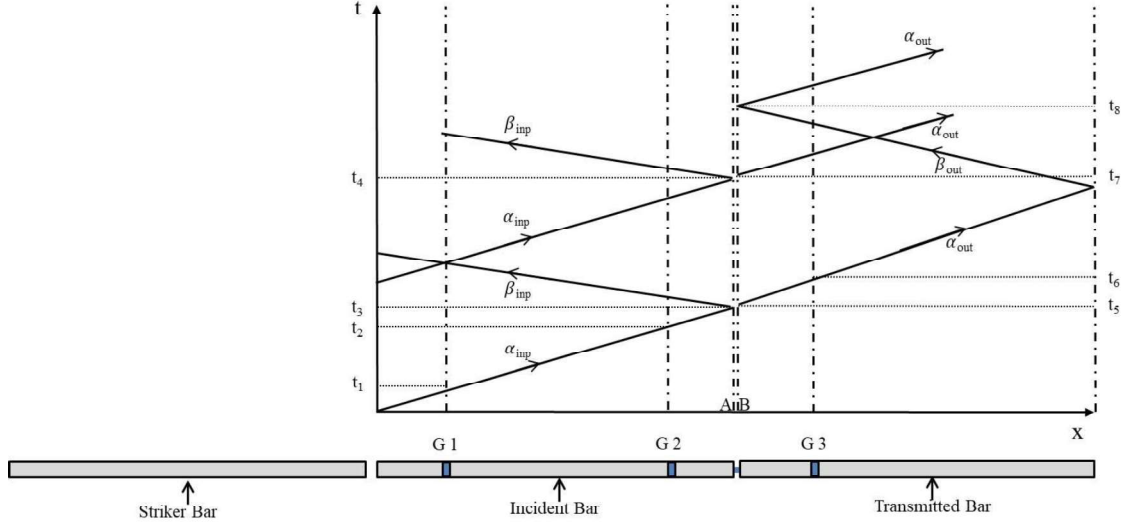


Fig.B1 Lagrangian diagram for stress wave propagation in long SHPB

A data analysis procedure, based on D'Alambert's solution of wave equations, is employed to determine the forward (α) and backward (β) travelling stress waves at the interfaces between two bars and specimen (marked by A and B). The procedure is given by the following algorithm :

For $t < t_4$,

$$\begin{cases} \alpha(x_A, t) = \sigma[x_{G1}, t - (t_3 - t_1)] \\ \beta(x_A, t) = \sigma[x_{G1}, t + (t_3 - t_2)] - \sigma[x_{G1}, t + (t_3 - t_2) - (t_2 - t_1)] \end{cases} \quad (B.1)$$

For $t \geq t_4$,

$$\begin{cases} \alpha(x_A, t) = \sigma[x_{G1}, t - (t_3 - t_1)] - \beta[x_A, t - (t_4 - t_3)] \\ \beta(x_A, t) = \sigma[x_{G2}, t + (t_3 - t_2)] - \{\sigma[x_{G1}, t + (t_3 - t_2) - (t_2 - t_1)] - \beta[x_A, t - 2(t_2 - t_1)]\} \end{cases} \quad (B.2)$$

For $t < t_7$,

$$\begin{cases} \alpha(x_B, t) = \sigma[x_{G3}, t + (t_6 - t_5)] \\ \beta(x_B, t) = 0 \end{cases} \quad (B.3)$$

For $t_7 \leq t < t_8$

$$\begin{cases} \alpha(x_B, t) = \sigma[x_{G3, t+}(t_6 - t_5)] + \alpha[x_B, t-(t_7 - t_5)] \\ \beta(x_B, t) = 0 \end{cases} \quad (B.4)$$

For $t \geq t_8$

$$\begin{cases} \alpha(x_B, t) = \sigma[x_{G3, t+}(t_6 - t_5)] + \alpha[x_B, t-(t_7 - t_5)] \\ \beta(x_B, t) = -\alpha[x_B, t-(t_8 - t_5)] \end{cases} \quad (B.5)$$

Once α and β at the two interfaces with the specimen are determined, the relative deformation and force acting on the specimen are obtained as:

$$\Delta u(t) = \int_0^t \left(\frac{\beta(x_A, t) - \alpha(x_A, t)}{\rho c} \right) dt - \int_0^t \left(\frac{\beta(x_B, t) - \alpha(x_B, t)}{\rho c} \right) dt \quad (B.6)$$

$$F(t) = \frac{1}{2} A_{\text{bar}} \{ [\alpha(x_A, t) + \beta(x_A, t)] + [\alpha(x_B, t) + \beta(x_B, t)] \} \quad (B.7)$$

Where ρ and c are the density and elastic wave speed of the bar, A_{bar} is the cross sectional area of the bar.

Reference:

- [1] J. Thorpe, Fatalities and destroyed civil aircraft due to bird strikes, 1912-2002, in: International Bird Strike Committee, 26th Meeting. Warsaw, Poland, 2003.
- [2] S. Georgiadis, A.J. Gunnion, R.S. Thomson, B.K. Cartwright, Bird-strike simulation for certification of the Boeing 787 composite moveable trailing edge, Composite Structures, 86 (2008) 258-268.
- [3] H. Kolsky, An investigation of the mechanical properties of materials at very high rates of loading, Proceedings of the Physical Society. Section B, 62 (1949) 676.
- [4] N.A. Fleck, W. Stronge, J. Liu, High strain-rate shear response of polycarbonate and polymethyl methacrylate, Proceedings of the Royal Society of London. A. Mathematical and Physical Sciences, 429 (1990) 459-479.
- [5] J. Richeton, S. Ahzi, K.S. Vecchio, F.C. Jiang, R.R. Adharapurapu, Influence of temperature and strain rate on the mechanical behavior of three amorphous polymers: Characterization and modeling of the compressive yield stress, Int J Solids Struct, 43 (2006) 2318-2335.
- [6] D. Rittel, Experimental investigation of transient thermoplastic effects in dynamic fracture, Int J Solids Struct, 37 (2000) 2901-2913.

- [7] M. Kendall, C. Siviour, Experimentally simulating high-rate behaviour: rate and temperature effects in polycarbonate and PMMA, *Philosophical Transactions of the Royal Society A: Mathematical, Physical and Engineering Sciences*, 372 (2014) 20130202.
- [8] R. Winter, Adiabatic shear of titanium and polymethylmethacrylate, *Philosophical Magazine*, 31 (1975) 765-773.
- [9] S. Satapathy, S. Bless, Deep punching PMMA, *Exp Mech*, 40 (2000) 31-37.
- [10] D. Rittel, A. Brill, Dynamic flow and failure of confined polymethylmethacrylate, *J Mech Phys Solids*, 56 (2008) 1401-1416.
- [11] P. Forquin, M. Nasraoui, A. Rusinek, L. Siad, Experimental study of the confined behaviour of PMMA under quasi-static and dynamic loadings, *Int. J. Impact Eng*, 40 (2012) 46-57.
- [12] X. Yao, Q. Han, X. Zhang, Experimental study on arc windshield of fighter subjected to bird impact, *Explosion and Shock Waves*, 25 (2005) 417.
- [13] X. Yao, L. Zhao, X. Liu, Numerical simulation for arc windshields of aircrafts subjected to bird impact, *Journal of Shanghai Jiaotong University*, (2004) 147-151.
- [14] G. Quino, Y. Chen, K.R. Ramakrishnan, F. Martínez-Hergueta, G. Zumpano, A. Pellegrino, N. Petrinic, Speckle patterns for DIC in challenging scenarios: rapid application and impact endurance, *Measurement Science and Technology*, 32 (2020) 015203.
- [15] L. Zhang, A. Pellegrino, D. Townsend, N. Petrinic, Temperature Dependent Dynamic Strain Localization and Failure of Ductile Polymeric Rods under Large Deformation, *International Journal of Mechanical Sciences*, 204 (2021) 106563.
- [16] D. Rittel, E. Hanina, G. Ravichandran, A note on the direct determination of the confining pressure of cylindrical specimens, *Exp Mech*, 48 (2008) 375-377.
- [17] L.M. Kachanov, *Foundations of the Theory of Plasticity*, North-Holland, 1971.
- [18] D. Rittel, A. Dorogoy, A methodology to assess the rate and pressure sensitivity of polymers over a wide range of strain rates, *J Mech Phys Solids*, 56 (2008) 3191-3205.
- [19] R. Gerlach, C. Kettenbeil, N. Petrinic, A new split Hopkinson tensile bar design, *Int. J. Impact Eng*, 50 (2012) 63-67.
- [20] F. De Cola, A. Pellegrino, C. Glößner, D. Penumadu, N. Petrinic, Effect of Particle Morphology, Compaction, and Confinement on the High Strain Rate Behavior of Sand, *Exp Mech*, 58 (2018) 223-242.
- [21] L. Zhang, A. Pellegrino, D. Townsend, N. Petrinic, Thermomechanical Constitutive Behaviour of a Near α Titanium Alloy over a Wide Range of Strain Rates: Experiments and Modelling, *International Journal of Mechanical Sciences*, 189 (2020) 105970.

782 [22] G. Quino, A. Pellegrino, V.L. Tagarielli, N. Petrinic, Measurements of the effects of
783 pure and salt water absorption on the rate-dependent response of an epoxy matrix,
784 Composites Part B: Engineering, 146 (2018) 213-221.

785 [23] Z. Li, J. Lambros, Strain rate effects on the thermomechanical behavior of polymers, Int
786 J Solids Struct, 38 (2001) 3549-3562.

787 [24] W. Blumenthal, C. Cady, G. Gray, Influence of temperature and strain rate on the
788 compressive behavior of PMMA and polycarbonate polymers, Bulletin of the American
789 Physical Society(USA), 46 (2001) 83-84.

790 [25] D. Drucker, W. Prager, H. Greenberg, Extended limit design theorems for continuous
791 media, Quarterly of applied mathematics, 9 (1952) 381-389.

792 [26] P. Bardia, R. Narasimhan, Characterisation of Pressure- sensitive Yielding in Polymers,
793 Strain, 42 (2006) 187-196.

794 [27] J. Richeton, S. Ahzi, K. Vecchio, F. Jiang, A. Makradi, Modeling and validation of the
795 large deformation inelastic response of amorphous polymers over a wide range of
796 temperatures and strain rates, Int J Solids Struct, 44 (2007) 7938-7954.

797 [28] W. Chen, G. Ravichandran, Dynamic compressive failure of a glass ceramic under
798 lateral confinement, J Mech Phys Solids, 45 (1997) 1303-1328.

799 [29] L. Zhang, D. Rittel, S. Osovski, Thermo-mechanical characterization and dynamic
800 failure of near α and near β titanium alloys, Mat Sci Eng a-Struct, 729 (2018) 94-101.

801 [30] A. Mulliken, M. Boyce, Mechanics of the rate-dependent elastic-plastic deformation of
802 glassy polymers from low to high strain rates, Int J Solids Struct, 43 (2006) 1331-1356.

803 [31] L. Zhang, X. Yao, S. Zang, Y. Gu, Temperature- and strain rate- dependent constitutive
804 modeling of the large deformation behavior of a transparent polyurethane interlayer, Polymer
805 Engineering & Science, 55 (2015) 1864-1872.

806 [32] L. Zhang, X. Yao, S. Zang, Q. Han, Temperature and strain rate dependent tensile
807 behavior of a transparent polyurethane interlayer, Materials & Design 65 (2015) 1181-1188.

808 [33] L. Zhang, X. Zhang, X. Yao, S. Zang, Experimental investigation on the tensile behavior
809 of a transparent polyurethane interlayer, International Journal of Materials Research, 106
810 (2015) 996-1001.

811 [34] S.Z. Tan, X.H. Yao, P. Yu, L.H. Zhang, S.G. Zang, Bird impact resistance analysis of
812 laminated glass structure, Transaction of Beijing Institute of Technology, 36 (2016) 170-173.

813 [35] Z. Liao, X. Yao, L. Zhang, M. Hossain, J. Wang, S. Zang, Temperature and strain rate
814 dependent large tensile deformation and tensile failure behavior of transparent polyurethane
815 at intermediate strain rates, Int. J. Impact Eng, 129 (2019) 152-167.

- 816 [36] E. Davies, S. Hunter, The dynamic compression testing of solids by the method of the
817 split Hopkinson pressure bar, *J Mech Phys Solids*, 11 (1963) 155-179.
- 818 [37] D. Gorham, P. Pope, J.E. Field, An improved method for compressive stress-strain
819 measurements at very high strain rates, *Proceedings of the Royal Society of London. Series A:*
820 *Mathematical and Physical Sciences*, 438 (1992) 153-170.
- 821 [38] S.M. Walley, J.E. Field, P. Pope, N. Safford, A study of the rapid deformation behaviour
822 of a range of polymers, *Philosophical Transactions of the Royal Society of London. Series A,*
823 *Mathematical and Physical Sciences*, 328 (1989) 1-33.
- 824 [39] B. Durand, F. Delvare, P. Bailly, D. Picart, A split Hopkinson pressure bar device to
825 carry out confined friction tests under high pressures, *Int. J. Impact Eng*, 88 (2016) 54-60.
- 826 [40] G.T. GRAY III, Classic split Hopkinson pressure bar testing, *ASM handbook*, 8 (2000)
827 462-476.

828